Composition of the plasmasphere and implications for refilling

Bill R. Sandel[1]

Received 3 May 2011; revised 2 June 2011; accepted 2 June 2011; published 20 July 2011.

[1] We compare measurements of He^+ by IMAGE/EUV with measurements of the local electron density n_e by IMAGE/RPI to derive new constraints on the relative abundance of He^+ in the plasmasphere. Analysis of 1067 pairs of He^+ and n_e determinations shows that the ratio of He^+ to n_e is much more variable early in the refilling process as compared to late, which may be related to interspecies differences in refilling rates. Further, the ratio is roughly constant with L for the periods studied, with a typical value of about 0.09.
Citation: Sandel, B. R. (2011), Composition of the plasmasphere and implications for refilling, *Geophys. Res. Lett.*, *38*, L14104, doi:10.1029/2011GL048022.

1. Introduction

[2] Earth's plasmasphere is a roughly torus-shaped region populated by cold plasma in dynamic equilibrium with the ionosphere. Its size, shape, and the distribution of plasma within it depend sensitively on the recent history of magnetic activity. Strong magnetospheric convection erodes the plasmasphere; during quiet times the plasmasphere expands toward an equilibrium "saturated" distribution. In establishing the equilibrium between the plasmasphere and the ionosphere, plasma flows both to and from the plasmasphere. A net flow into the plasmasphere is often called "refilling." Refilling of the plasmasphere has been a topic of active study since the discovery of the plasmasphere more than forty years ago. However, most previous studies have used either in situ measurements by satellites, or ground-based measurements, which typically sample the density along a field line. Building a complete picture in local time and L then necessarily required combining measurements from many times, often made under different magnetic conditions.

[3] Here we use He^+ abundance measurements by IMAGE/EUV [*Sandel et al.*, 2000, 2003] together with determinations of the local electron density by IMAGE/RPI [*Reinisch et al.*, 2000; *Green et al.*, 2000] to infer the relative abundances of the two species. During the summer of 2001, the IMAGE satellite reached apogee at high northern latitudes, and EUV imaged the full plasmasphere. Approximately one-half orbit before and after apogee, IMAGE passed through the plasmasphere, and RPI measured the local electron density n_e. Thus we have the opportunity to compare in situ measurements of electron density with remote measurements He^+ made in the same region and separated in time by ~7 hours.

2. Observations

[4] Figure 1 shows an example of an EUV image used in our analysis. We summed the native 10-min exposures transmitted from IMAGE to improve the signal-to-noise ratio; this image is a sum of five consecutive native EUV images from a single apogee pass, with background subtracted. The number of native images summed to form the composites used in the analysis ranged from two to ten; the average number was 7.2. To reduce the effects of smearing caused by corotation, before summing we projected each 10-min image to the plane of the magnetic equator using the Earth-fixed magnetic longitude system as the azimuthal coordinate [*Sandel et al.*, 2003]. It is likely that sub-corotation of the plasmasphere relative to the magnetic longitude system [*Sandel et al.*, 2003; *Burch et al.*, 2004; *Galvan et al.*, 2010] introduces a small amount of residual smearing. For an 80-minute integration and 10% sub-corotation, the differential motion would be ~0.15 R_E at L = 4, about half the size of our sampling window of 0.3 R_E (as discussed later), and hence negligible.

[5] We use IMAGE/RPI electron density measurements made using passive dynamic spectra. Values of the local plasmaspheric electron density are derived along the IMAGE orbit from RPI measurements of the upper hybrid band, and are accurate to a few percent [*Benson et al.*, 2004]. The RPI measurements that we use are typically reported at intervals of approximately 2–5 min along the orbit. This spacing corresponds to a spacing in L of 0.1–0.5, depending on position in the orbit. This is dense enough to permit an accurate comparison with EUV measurements, given that EUV measures a line-of-sight abundance. For this work, it is unnecessary to include the possibility of a variation of n_e along the field line. Information on this latitude variation is available from RPI for some time intervals [*Reinisch et al.*, 2004; *Tu et al.*, 2006]. The variation is pronounced at high latitudes. However, for the observing geometry that we encounter here, the main contribution of light along the EUV line of sight comes from near the magnetic equator. It is here that the value of L along the line of sight is minimum, and hence where the He^+ abundance reaches its maximum value along the line of sight. Figure 2 of *Sandel et al.* [2003] shows that, under typical conditions, about half the brightness comes from within 0.5 R_E of the magnetic equator. Figure A1 of *Gallagher et al.* [2005] also illustrates this situation. Moreover, by integrating the RPI-derived electron density given by *Reinisch et al.* [2004] for representative EUV observing geometries, we find that including the variation of electron density with latitude along the field line amounts to an effect of only a few

[1]Lunar and Planetary Laboratory, University of Arizona, Tucson, Arizona, USA.

0094-8276/11/2011GL048022

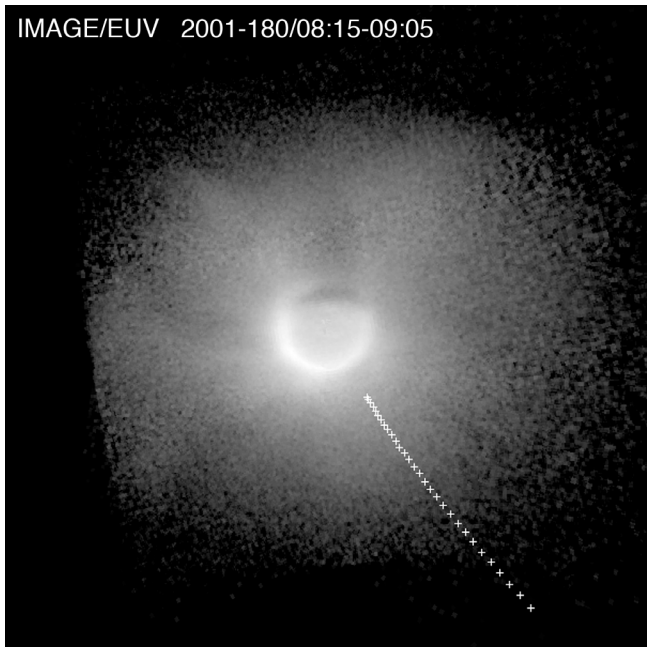

Figure 1. An example of the EUV images used as a starting point for comparing He^+ and electron abundances. This image shows the brightness of the 30.4-nm resonance line of He^+ in the plasmasphere. It is a sum of five 10-minute native EUV images. The white crosses mark the locations of RPI determinations of the local electron density used in our analysis. The image and pluses are shown projected to the plane of the magnetic equator. The azimuthal coordinate is magnetic longitude, with 0 to the right. The image frame extends ±8 R_E from the center of Earth in both directions. Earth's shadow, slightly smeared by summation in magnetic longitude, extends toward the top of the frame.

percent for the portions of the plasmasphere of interest here. Therefore it is unnecessary to include this effect routinely in our analysis.

[6] EUV and RPI measure fundamentally different quantities: the brightness of an EUV image is proportional to the column abundance of He^+ along lines of sight corresponding to each pixel in the image, whereas we use RPI measurements of the local electron density along the orbit. Comparing the two measurements in a meaningful way requires establishing a common basis for the two disparate sets of observations. At least two approaches are available:

[7] 1. We could invert the EUV images using the methods described by *Gallagher et al.* [2005] or *Gurgiolo et al.* [2005] to estimate volume abundances of He^+, and compare these directly with electron densities from RPI.

[8] 2. We could compute line-of-sight column abundances of electrons based on RPI measurements, and compare these directly with He^+ column abundances from EUV.

[9] In both cases, approximations are required to accommodate the differences between two- and three-dimensional situations. The techniques for estimating local abundances from EUV images rely on assuming that the abundance of He^+ along a field line is constant. This same assumption leads to a convenient way of computing line-of-sight electron column abundances from local measurements. Because image inversion is typically not noise-free, here we choose the second alternative. For the line of sight integration of electron abundance, we assume constant electron density along a field line, and we explicitly neglect azimuthal variations by assuming that each RPI measurement applies to the meridian plane in the projected image that is sampled by the particular EUV line of sight. We discuss uncertainties introduced by these approximations below.

[10] The locations of the n_e measurements establish the positions in the EUV image where our comparison is possible. To define these locations, we project onto the EUV image the locations of the n_e measurements from the preceding and following passes through the plasmasphere. The white crosses in Figure 1 mark these locations. We then sample the EUV brightness at the position of each n_e measurement by averaging over a square of 3 × 3 pixels, equivalent to about 0.3 × 0.3 R_E. We convert this brightness to a He^+ column abundance using the sensitivity of EUV and the solar flux at 30.4 nm for the time of the image as documented by *Gallagher et al.* [2005]. These column abundances are shown in Figure 2 (bottom) for our example image.

[11] For each [L, magnetic longitude] pair in the image sampled in this way, we have a corresponding n_e measurement. Using the approximations outlined above, we have enough information to define the electron distribution along the EUV line of sight. We then integrate this distribution along the line of sight to find the column abundance of electrons, a quantity directly comparable to the column abundance of He^+ already determined. Figure 2 shows the result, computed for each sampled point in the

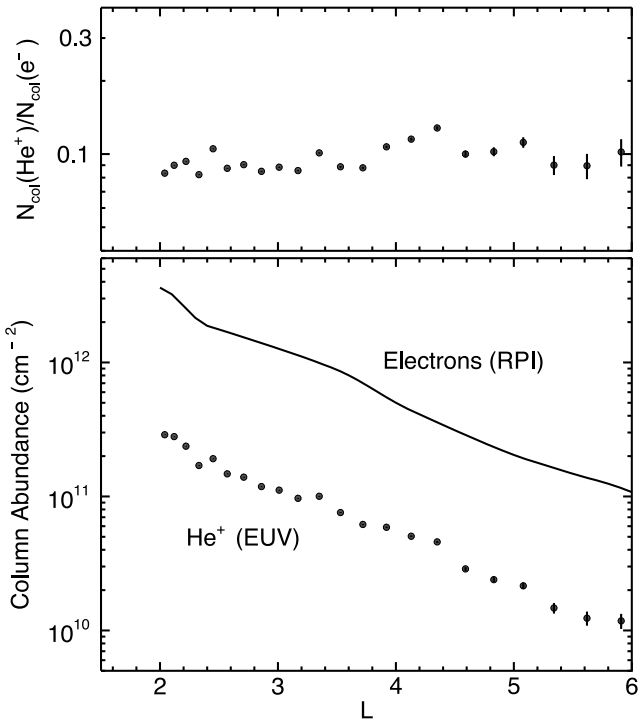

Figure 2. (bottom) Column abundances of He^+ from EUV (points) and electrons from RPI (solid line). In this example, the plasmasphere is near its saturated state and the plasmapause is not clearly defined. (top) The ratio of the column abundances in Figure 2 (bottom).

Table 1. Periods of Observations

Period	Days	Dates	Orbits
A	2001/128–132	8 May–12 May	9
B	2001/167–175	16 Jun–24 Jun	15
C	2001/177–181	26 Jun–30 Jun	8

image for which sufficient spatial coverage is available in the electron abundance measurements. With this information in hand, computing the ratio of the two column abundances (Figure 2, top) is straightforward.

[12] In this example, this ratio is roughly constant with L. This is typically (though not invariably) true for the cases that we have examined. The uncertainties indicated by the error bars include the probable error in the photometric measurements derived from Poisson counting statistics and then propagated using standard techniques. The uncertainties increase with L because the lower brightness at higher values of L results in fewer detected photons, and hence poorer statistical accuracy. Systematic errors such as those arising from errors in calibration, estimated to be ±20%, are not included. Given our present focus, such errors are of secondary importance because they move the He^+ abundance curve up or down without affecting its shape. The uncertainty in n_e is small compared to other sources of error, and we disregard it in our calculation.

[13] Other potentially important sources of error arise in the processing needed to compare EUV and RPI results. To assure photometric accuracy we exclude EUV observations near Earth's shadow. Our computations of electron column abundances could be biased by azimuthal non-uniformity in n_e. To guard against this possibility, we exclude times for which EUV images reveal significant azimuthal structures in the region probed by RPI. Doing so also helps to limit errors in placement arising from sub-corotation. For 10% sub-corotation over a 7-h gap between EUV and RPI measurements, the differential azimuthal motion would be ~0.7 R_E at $L = 4$, or about twice the size of our sampling window. Finally, we note that the character of IMAGE's orbit leads to nearly radial sampling paths when projected onto the plane of the magnetic equator, thus confining each set of n_e measurements to a small range of magnetic longitudes.

3. Results

[14] We have applied these techniques to observations during the three periods shown in Table 1. Each of these began with a moderate erosion event, which was followed by a time of relatively low geomagnetic activity. During the low-activity periods, the plasmasphere refilled toward its "saturated" condition. We selected the pairs of EUV and RPI observations that meet the criteria already described, and processed them as above. Table 1 shows the number of composite EUV images available for each observation period. For some apogees, n_e measurements during both the preceding (ascending) and the following (descending) plasmasphere passes were available; in this case, we used both sets of n_e observations. From the 32 orbits in Table 1, we have identified 1067 useful pairs of He^+ and corresponding n_e determinations.

[15] Figure 3 (bottom) shows the resulting ratios for each of the 1067 determinations. This full data set includes times of most active refilling as well as nearly-saturated conditions. Most of the measurements relate to positions in the range $2.0 \le L \le 4.5$. The best fit line (solid) shows that the ratio is nearly constant with L at a value of about 0.09. Substantial scatter is present in the ratio, which ranges from ~0.05 to ~0.3 over essentially all values of L. Figure 3 (top) shows a subset of the data drawn from Figure 3 (bottom) by selecting the later portions of the study periods. Therefore these data relate to times for which the plasmasphere was approaching its equilibrium distribution. The most striking difference between the two sets is the much lower scatter in the ratio in Figure 3 (top), i.e., for times nearing saturation. At some values of L the He^+ signal is lower early in the refilling period, but the error bars show that this cannot account for the higher scatter at these times.

[16] The ratio of He^+/n_e computed as described by *Craven et al.* [1997] is shown by the dashed line in Figures 3 (top) and 3 (bottom). Their results are derived from measurements by the Retarding Ion Mass Spectrometer on Dynamics Explorer I made during more than three years beginning near a peak in solar activity and extending into the declining phase. Our present measurements refer to a period near a

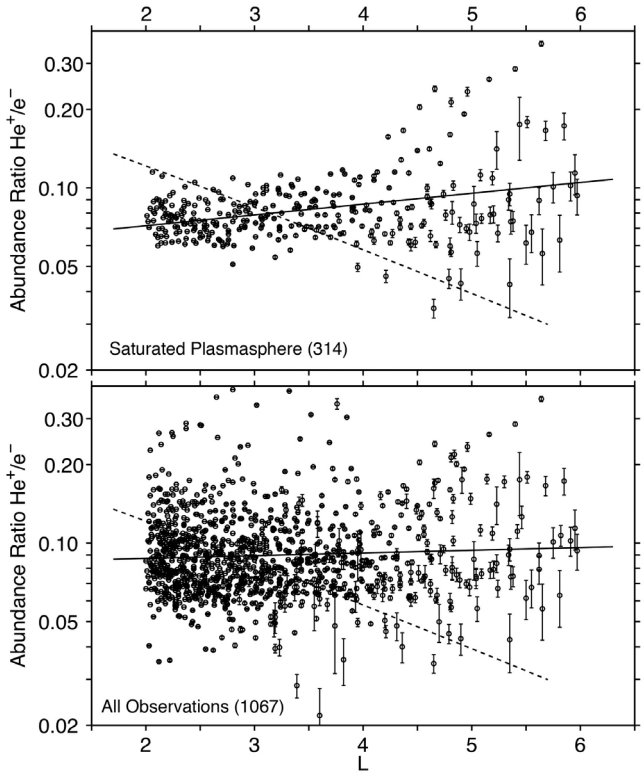

Figure 3. (bottom) The ratio of He^+ abundance (from IMAGE/EUV) and electron abundance (from IMAGE/RPI) at the same locations within the plasmasphere. (top) A subset of the data in the lower panel, chosen from times when the plasmasphere was at or near its saturation level. In Figures 3 (bottom) and 3 (top), the solid line is the best-fit straight line in the least-squares sense through the logarithm of the measured ratios. The dashed line is the ratio expected on the basis of the relation reported by *Craven et al.* [1997] for a solar F10.7 flux appropriate for the time of the observations.

peak in solar activity. (*Craven et al.* [1997] provide an expression for $[He^+]/[H^+]$; we have converted this to the plotted quantity under the approximation that He^+ and H^+ are the only positive ions present.)

4. Discussion

[17] In Figure 3, the slope of the best fit to the measurements differs significantly from the behavior expected using the relation from *Craven et al.* [1997]. Their observations span a much more extensive sample of times and geomagnetic and solar conditions than our present analysis, and so are more likely to represent typical conditions. Nonetheless it is important to understand this difference, because it is often desirable to use EUV measurements of He^+ as a proxy for the total plasma abundance in the plasmasphere. For example, we note that using our new estimate of the radial variation instead of that of *Craven et al.* [1997] improves the comparison in Figure 3 of *Sandel and Denton* [2007] of their refilling rates with those inferred from previous measurements and models. In that work, Sandel and Denton used the relation shown by the dashed line in Figure 3 to estimate the He^+ refilling rate from measurements and models of other quantities reported by other authors. Using the best-fit solid line in Figure 3 instead of the dashed line to re-estimate these He^+ refilling rates reduces the values at low L, where they were too high, and raises them at large L, where they were too low.

[18] Further, a better understanding of interspecies differences in the ionospheric outflow responsible for populating the plasmasphere should help to clarify the details of the regulating mechanisms. Figure 3 shows that early in the refilling period the scatter in the ratio is roughly equally distributed about the most likely value. This suggests that the controlling mechanism could be capable of either suppressing or enhancing He^+ outflow in comparison with some typical value. Late in the refilling period, scatter persists at $L > 4$ This may reflect the longer time needed for these more distant regions to reach equilibrium.

[19] **Acknowledgments.** We thank P. A. Webb for providing the n_e measurements in a convenient form, and the reviewers for helpful comments. The IMAGE Mission was supported under NASA contract NAS5-96020 to SwRI. Additional work at The University of Arizona was supported under NASA grant NNX07AG46G from the Heliospheric Guest Investigator Program.

[20] The Editor thanks Joseph Borovsky and David Galvan for their assistance in evaluating this paper.

References

Benson, R. F., P. A. Webb, J. L. Green, L. Garcia, and B. W. Reinisch (2004), Magnetospheric electron densities inferred from upper-hybrid band emissions, *Geophys. Res. Lett.*, *31*, L20803, doi:10.1029/2004GL020847.

Burch, J. L., J. Goldstein, and B. R. Sandel (2004), Cause of plasmasphere corotation lag, *Geophys. Res. Lett.*, *31*, L05802, doi:10.1029/2003GL019164.

Craven, P. D., D. L. Gallagher, and R. H. Comfort (1997), Relative concentration of He^+ in the inner magnetosphere as observed by the DE 1 retarding ion mass spectrometer, *J. Geophys. Res.*, *102*, 2279–2289, doi:10.1029/96JA02176.

Gallagher, D. L., M. L. Adrian, and M. W. Liemohn (2005), Origin and evolution of deep plasmaspheric notches, *J. Geophys. Res.*, *110*, A09201, doi:10.1029/2004JA010906.

Galvan, D. A., M. B. Moldwin, B. R. Sandel, and G. Crowley (2010), On the causes of plasmaspheric rotation variability: IMAGE EUV observations, *J. Geophys. Res.*, *115*, A01214, doi:10.1029/2009JA014321.

Green, J. L., et al. (2000), Radio plasma imager simulations and measurements, *Space Sci. Rev.*, *91*, 361–389.

Gurgiolo, C., B. R. Sandel, J. D. Perez, D. G. Mitchell, C. J. Pollock, and B. A. Larsen (2005), Overlap of the plasmasphere and ring current: Relation to subauroral ionospheric heating, *J. Geophys. Res.*, *110*, A12217, doi:10.1029/2004JA010986.

Reinisch, B. W., et al. (2000), The Radio Plasma Imager investigation on the IMAGE spacecraft, *Space Sci. Rev.*, *91*, 319–359.

Reinisch, B. W., X. Huang, P. Song, J. L. Green, S. F. Fung, V. M. Vasyliunas, D. L. Gallagher, and B. R. Sandel (2004), Plasmaspheric mass loss and refilling as a result of a magnetic storm, *J. Geophys. Res.*, *109*, A01202, doi:10.1029/2003JA009948.

Sandel, B. R., and M. H. Denton (2007), Global view of refilling of the plasmasphere, *Geophys. Res. Lett.*, *34*, L17102, doi:10.1029/2007GL030669.

Sandel, B. R., et al. (2000), The Extreme Ultraviolet Imager investigation for the IMAGE Mission, *Space Sci. Rev.*, *91*, 197–242.

Sandel, B. R., J. Goldstein, D. L. Gallagher, and M. Spasojević (2003), Extreme Ultraviolet Imager observations of the structure and dynamics of the plasmasphere, *Space Sci. Rev.*, *109*, 25–46, doi:10.1023/B:SPAC.0000007511.47727.5b.

Tu, J., P. Song, B. W. Reinisch, J. L. Green, and X. Huang (2006), Empirical specification of field-aligned plasma density profiles for plasmasphere refilling, *J. Geophys. Res.*, *111*, A06216, doi:10.1029/2005JA011582.

B. R. Sandel, Lunar and Planetary Laboratory, University of Arizona, 1541 E. University Blvd., Tucson, AZ 85721, USA. (sandel@arizona.edu)